

# Magnetization dynamics induced by in-plane currents in ultrathin magnetic nanostructures

Kyoung-Whan Kim<sup>1</sup>, Soo-Man Seo<sup>2</sup>, Jisu Ryu<sup>1</sup>, Kyung-Jin Lee<sup>2,3,4,\*</sup> and Hyun-Woo Lee<sup>1†</sup>  
<sup>1</sup>*PCTP and Department of Physics, Pohang University of Science and Technology, Pohang, 790-784, Korea*  
<sup>2</sup>*Department of Materials Science and Engineering, Korea University, Seoul 136-701, Korea*  
<sup>3</sup>*Center for Nanoscale Science and Technology, National Institute of Standards and Technology, Gaithersburg, Maryland 20899-8412, USA*  
<sup>4</sup>*Maryland Nanocenter, University of Maryland, College Park, MD 20742, USA*

(Dated: November 8, 2018)

Ultrathin magnetic systems have properties qualitatively different from their thicker counterparts, implying that different physics governs their properties. We demonstrate that various such properties can be explained naturally by the Rashba spin-orbit coupling in ultrathin magnetic systems. This work will be valuable for the development of next generation spintronic devices based on ultrathin magnetic systems.

Electric control of magnetic systems carries high potential towards device applications [1, 2] such as magnetic memory and logic. Spin-transfer torque (STT) [3, 4] is an efficient way to achieve the electric control of magnetic nanostructures. In view of device applications, magnetic nanostructures such MgO-based magnetic tunnel junctions are superior to silicon-based nanostructures in the simultaneous realization of nonvolatility and speed, but are estimated to require 100 times more energy [5] than silicon-based CMOS devices to write an information bit. This energy cost problem limits scope of device applications based on magnetic nanostructures. Since the writing energy decreases as a magnetic layer in magnetic nanostructures becomes thinner [2], properties of ultrathin magnetic layers are under intense investigation [6].

While the magnetization switching for the information writing is conventionally achieved by a current perpendicular to a magnetic layer, a recent experiment [7] found that an *in-plane* current can also switch the uniform magnetization of an ultrathin ( $\approx 1$  nm) magnetic layer (Co) sandwiched between a heavy metal layer (Pt) and an oxide layer ( $\text{AlO}_x$ ) (Fig. 1). Since the cross-sectional area (in  $yz$ -plane) for the in-plane current can be orders of magnitude smaller than the cross-sectional area (in  $xy$ -plane) for the perpendicular current, this alternative switching scheme may reduce the current required for the switching and the switching energy. It was also reported that the magnetic domain wall (DW) in the ultrathin magnetic layer moves as fast as 400 m/s [8] when in-plane current is supplied. This velocity is about 4 times higher than the highest velocity reported for thicker magnetic layers [9]. Thus the in-plane current effects on ultrathin magnetic systems open an attractive alternative path towards powerful spintronic devices.

Ultrathin magnetic systems are interesting in view of fundamental science as well. Various features of ultrathin magnetic systems cannot be explained by existing theoretical knowledge learned from measurements on thicker counterparts; for example (i) magnetization switching by in-plane current [7] instead of perpendic-

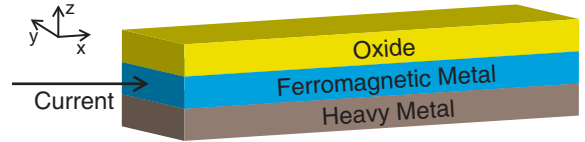


FIG. 1: (color online) Schematic structure of ultrathin magnetic nanostructure, where an ultrathin ( $\approx 1$  nm) ferromagnetic layer is sandwiched between a heavy metallic layer and an insulating oxide layer. Examples include Pt/Co/ $\text{AlO}_x$  and Ta/CoFeB/MgO.

ular current, (ii) DW motion against the electron flow direction [8, 10] instead of along it, and (iii) anomalously high DW speeds [8]. These anomalies imply that ultrathin magnetic systems are not mere thin limits of thicker counterparts but are qualitatively different systems governed by different physics. A clear understanding of their core physics will be highly valuable for developments of spintronic devices.

Since the upper and lower layers of the ultrathin magnetic layer are made of quite different materials (Fig. 1), the ultrathin magnetic layer has the structural asymmetry. Here we demonstrate theoretically that if the Rashba spin-orbit coupling (RSOC) [11] due to the asymmetry is sufficiently strong, all the anomalies (i), (ii), and (iii) can be explained naturally. To be specific, we show that the in-plane current gives rise to a torque proportional to  $\alpha_R \mathbf{m} \times [\mathbf{m} \times (\hat{\mathbf{z}} \times \mathbf{j}_e)]$  [12], where  $\alpha_R$  is the parameter describing the strength of the RSOC,  $\mathbf{j}_e$  is the in-plane current density in the ultrathin magnetic layer,  $\hat{\mathbf{z}}$  is the unit vector perpendicular to the layer, and  $\mathbf{m}$  is the unit vector along the magnetization in the ultrathin magnetic layer. Since this torque has the same form as the Slonczewski STT [3] in magnetic multilayers, we call it Slonczewski-like STT (SL-STT). We demonstrate that the SL-STT explains all three anomalies naturally. Recently an experiment [13] proposed that the anomaly (i) may arise due to the spin Hall effect (SHE) in the heavy metal layer. Here we demonstrate that the SHE alone

cannot explain the anomalies (ii) and (iii).

First, we demonstrate that RSOC generates the SL-STT. Conduction electrons in the ultrathin ferromagnetic layer can be described by the Hamiltonian,

$$H = \frac{\mathbf{p}_{\text{op}}^2}{2m_e} + J_{\text{ex}}\boldsymbol{\sigma} \cdot \mathbf{m} + \frac{\alpha_{\text{R}}}{\hbar}(\boldsymbol{\sigma} \times \mathbf{p}_{\text{op}}) \cdot \hat{\mathbf{z}} + H_{\text{rel}}, \quad (1)$$

where  $\mathbf{p}_{\text{op}}$  is the momentum operator,  $m_e$  is the electron mass,  $J_{\text{ex}} (> 0)$  is the exchange energy, and  $\boldsymbol{\sigma}$  is the Pauli matrix. The third term in Eq. (1) is the RSOC Hamiltonian and the last term describes spin relaxation processes such as electron scattering. When expressed in terms of the kinematic velocity operator  $\mathbf{v}_{\text{op}} \equiv \mathbf{p}_{\text{op}}/m_e + (\alpha_{\text{R}}/\hbar)\hat{\mathbf{z}} \times \boldsymbol{\sigma}$ , Eq. (1) becomes  $H = m_e\mathbf{v}_{\text{op}}^2/2 + J_{\text{ex}}\boldsymbol{\sigma} \cdot \mathbf{m} + H_{\text{rel}}$ , where a trivial  $c$ -number has been neglected. Due to the strong exchange energy  $J_{\text{ex}}$ , which is the largest energy scale affecting the spin dynamics in conventional metallic ferromagnets (such as Co or Fe), electrons in energy bands still carry largely majority and minority spin directions. However within each of these bands, the individual spins and the net spin are not necessarily collinear with the magnetization due to tilting of the spins by RSOC. In the following, we treat the electrons on the majority and minority sheets of the Fermi surface separately, but need to treat each spin density as a vector  $\mathbf{s}_{\pm} \equiv \langle \boldsymbol{\sigma} \rangle_{\pm}$ , since it is not aligned with the magnetization. Here  $\langle \cdots \rangle_{\pm}$  denotes local average over majority/minority electrons. The spin continuity equation determined by  $H$  allows one to derive the Bloch equation for  $\mathbf{s}_{\pm}$ ,

$$\frac{\partial \mathbf{s}_{\pm}}{\partial t} + \nabla \cdot \mathcal{J}_{\pm} = -\frac{\mathbf{s}_{\pm}}{\tau_{\text{ex}}} \times \left[ \mathbf{m} + \frac{2\alpha_{\text{R}}m_e\tau_{\text{ex}}}{\hbar^2}(\mathbf{v}_{\pm} \times \hat{\mathbf{z}}) \right] + \langle \boldsymbol{\Gamma} \rangle_{\pm}, \quad (2)$$

where  $\tau_{\text{ex}} \equiv \hbar/2J_{\text{ex}}$ ,  $\mathbf{v}_{\pm} = \langle \mathbf{v}_{\text{op}} \rangle_{\pm}$ , and  $\boldsymbol{\Gamma} = [\boldsymbol{\sigma}, H_{\text{rel}}]/i\hbar$ , and the spin-current tensor density  $\mathcal{J}_{\pm} = \mathbf{v}_{\pm} \otimes \mathbf{s}_{\pm}$ . The approximation  $\langle (\boldsymbol{\sigma})_i (\mathbf{v}_{\text{op}})_j + (\mathbf{v}_{\text{op}})_j (\boldsymbol{\sigma})_i \rangle_{\pm} = 2(\mathbf{s}_{\pm})_i (\mathbf{v}_{\pm})_j$  is used in Eq. (2) [14]. Recalling that STT is determined by the transverse component  $\delta \mathbf{s}_{\pm}$  of  $\mathbf{s}_{\pm}$  perpendicular to  $\mathbf{m}$ , it is useful to separate  $\mathbf{s}_{\pm}$  into longitudinal and transverse components,  $\mathbf{s}_{\pm} = \mp n_{\pm} \mathbf{m} + \delta \mathbf{s}_{\pm}$ , where  $n_{\pm} = \mp \mathbf{s}_{\pm} \cdot \mathbf{m}$  is the longitudinal spin accumulation. One then makes the relaxation time approximation [15],  $\langle \boldsymbol{\Gamma} \rangle_{\pm} = -\delta \mathbf{s}_{\pm} / \tau_{\text{sr}}$ , where  $\tau_{\text{sr}}$  is the transverse spin relaxation time. In this approximation, the relaxation of the longitudinal spin component is neglected since the transverse relaxation is much faster in conventional metallic ferromagnets and also the longitudinal spin component does not affect the STT. When  $\mathbf{v}_{\pm}$  is assumed to be homogeneous [16] within the magnetic layer, one can determine from Eq. (2) the following approximate solution for  $\delta \mathbf{s}_{\pm}$ ,

$$\delta \mathbf{s}_{\pm} = \pm n_{\pm} \tau_{\text{ex}} \frac{(\beta + \mathbf{m} \times)}{1 + \beta^2} \left[ D_t^{\pm} \mathbf{m} + \frac{2\alpha_{\text{R}}m_e}{\hbar^2} \mathbf{m} \times (\mathbf{v}_{\pm} \times \hat{\mathbf{z}}) \right], \quad (3)$$

where  $\beta = \tau_{\text{ex}}/\tau_{\text{sr}}$  and  $D_t^{\pm} = \partial_t + \mathbf{v}_{\pm} \cdot \nabla$ . Corrections to this solution are of higher order in  $\tau_{\text{ex}}$  and may be neglected in the strong  $J_{\text{ex}}$  limit. Finally from the relation  $\mathbf{T} = \mu_B \tau_{\text{ex}}^{-1} \mathbf{m} \times \delta \mathbf{s}$  between STT  $\mathbf{T}$  and the total transverse spin density  $\delta \mathbf{s} = \delta \mathbf{s}_+ + \delta \mathbf{s}_-$ , one obtains the Landau-Lifshitz-Gilbert equation  $\partial \mathbf{M} / \partial t = -\gamma_0 \mathbf{M} \times \mathbf{H}_{\text{eff}} + (\alpha_0/M_s) \mathbf{M} \times \partial \mathbf{M} / \partial t + \mathbf{T}$ , where  $\mathbf{H}_{\text{eff}}$  is a sum of an external magnetic field and effective magnetic fields due to magnetic anisotropy and magnetic exchange energy.  $\mathbf{M} = M_s \mathbf{m}$  is the magnetization and  $M_s$  is saturation magnetization in the ultrathin magnetic layer. After grouping together terms of the same structure, one obtains

$$\begin{aligned} \frac{\partial \mathbf{M}}{\partial t} = & -\gamma \mathbf{M} \times \left( \mathbf{H}_{\text{eff}} + \mathbf{H}_{\text{R}} - \frac{\beta}{M_s} \mathbf{M} \times \mathbf{H}_{\text{R}} \right) \\ & + \frac{\alpha}{M_s} \mathbf{M} \times \frac{\partial \mathbf{M}}{\partial t} + \frac{\mu_B P}{eM_s(1 + \beta^2)} (\mathbf{j}_e \cdot \nabla) \mathbf{M} \\ & - \frac{\beta \mu_B P}{eM_s^2(1 + \beta^2)} \mathbf{M} \times (\mathbf{j}_e \cdot \nabla) \mathbf{M}. \end{aligned} \quad (4)$$

$$\mathbf{H}_{\text{R}} = \frac{\alpha_{\text{R}} m_e P}{\hbar e M_s (1 + \beta^2)} (\hat{\mathbf{z}} \times \mathbf{j}_e), \quad (5)$$

where  $\mathbf{H}_{\text{R}}$  is the additional effective magnetic field due to RSOC,  $\mathbf{j}_e = -e(n_+ \mathbf{v}_+ + n_- \mathbf{v}_-)$ , and  $P \mathbf{j}_e = -e(n_+ \mathbf{v}_+ - n_- \mathbf{v}_-)$ . Note that the first and fourth terms on the right-hand-side of Eq. (4) contain the renormalized gyromagnetic ratio  $\gamma$  and the renormalized Gilbert damping  $\alpha$  given by  $\gamma_0/\gamma = 1 + (n_+ - n_-)/[M_s(1 + \beta^2)]$ , and  $\gamma\alpha/\gamma_0 = \alpha_0 + \beta(n_+ - n_-)/[M_s(1 + \beta^2)]$ . The last and second to the last terms are the nonadiabatic STT [15, 17] and the adiabatic STT [18]. These four terms govern the magnetization dynamics in thicker magnetic systems.

The second and third terms are additional STTs due to RSOC and may have sizable magnitude only in ultrathin magnetic systems since  $\alpha_{\text{R}}$  decays as the magnetic layer becomes thicker. The second term  $-\gamma \mathbf{M} \times \mathbf{H}_{\text{R}}$  has the same structure as the first term and thus we call it field-like STT (FL-STT). The FL-STT was derived previously [19, 20] and Ref. [21] reported its experimental confirmation. The FL-STT alone, however, can explain none of the anomalies, as we demonstrated recently [22]. The third term is the very SL-STT that this calculation aims to derive.

Next we explain the anomalies in terms of the SL-STT. Explanation for the anomaly (i) is trivial. Recalling that the SL-STT due to the in-plane current has the exactly same structure as the Slonczewski STT [3] due to the perpendicular current in metallic spin valve systems and that the Slonczewski STT induces the magnetization switching in the spin valve systems, it is easy to understand that the in-plane current can induce the magnetization switching through the action of the SL-STT.

The anomalies (ii) and (iii) are less trivial to explain since they arise from the combined action of the SL- and FL-STTs. To explain the anomalies, we begin with

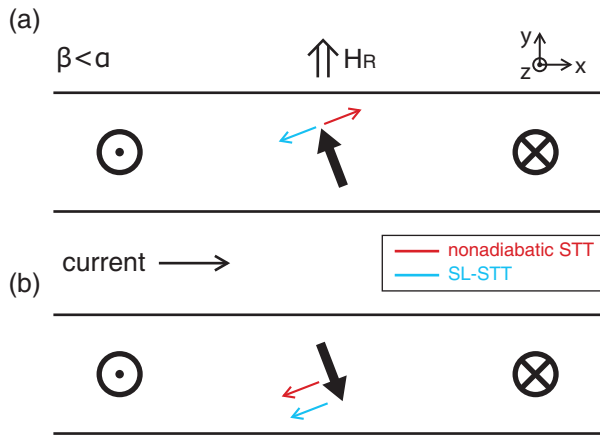


FIG. 2: (color online) Two possible structures of the Bloch DW when the current flows to the right and  $\alpha > \beta$  [23]. Thick and thin arrows represent the directions of  $\mathbf{m}$  and STTs, respectively. Note that the direction of  $\mathbf{m}$  deviates from  $\pm\hat{y}$ , which is a generic feature of a moving DW [15, 17] with  $\alpha \neq \beta$ .

two possible structures of the Bloch DW (Fig. 2) in ultrathin magnetic systems (such as Pt/Co/AlO<sub>x</sub> [8, 21]) with the perpendicular magnetic anisotropy. In the absence of RSOC and when  $\mathbf{j}_e$  is not large enough to cause the DW structural instability (Walker breakdown) [17], the two structures are equivalent in term of both stability and dynamics (same DW velocity  $v_{\text{DW}}$ ). The first effect of RSOC is to break the dynamic equivalence; at the DW center in Fig. 2(a)/(b), the SL-STT is anti-parallel/parallel to the nonadiabatic STT, effectively cancelling/enlarging the effect of the nonadiabatic STT. Recalling that the nonadiabatic STT determines  $v_{\text{DW}}$  [15, 17], this implies that the SL-STT reduces/increases  $v_{\text{DW}}$ . When RSOC is sufficiently strong, it is even possible that the SL-STT over-cancels the nonadiabatic STT in Fig. 2(a), so that  $v_{\text{DW}}$  reverses its sign. When RSOC is even stronger,  $v_{\text{DW}}$  will be large with the reversed sign, implying that the DW in Fig. 2(a) moves *fast against* the electron flow direction. By the way, the FL-STT does not affect  $v_{\text{DW}}$  [22] since it is perpendicular to the nonadiabatic STT at the DW center. The second effect of RSOC is to break the stability equivalence. The effect of the FL-STT on the stability can be understood from the direction of the effective field  $\mathbf{H}_R$ . Since the effective energy density  $-\mathbf{H}_R \cdot \mathbf{M}$  is negative/positive at the DW center for the DW structure in Fig. 2(a)/(b), the FL-STT makes the DW structure in Fig. 2(a) more stable than the other structure. Moreover when  $\mathbf{H}_R$  is sufficiently strong, the DW structure in Fig. 2(b) becomes unstable and evolves to the stable DW structure in Fig. 2(a) [22]. By the way, the SL-STT has much weaker effect on the stability than the FL-STT since, according to Eq. (4), the SL-STT is smaller than the FL-STT in magnitude by factor  $\beta$  and this nonadiabaticity parameter  $\beta$  is known [15] to be smaller than

1. Then combining the above information, we find that there is only one stable DW structure [Fig. 2(a)] when RSOC is sufficiently strong and that it moves fast against the electron flow direction, explaining both the anomalies (ii) and (iii).

The experiment [8], which reported the anomalies (ii) and (iii), provides sufficient information to test this explanation. According to Eq. (4), the magnitude of the SL-STT is  $\gamma\beta|\mathbf{M} \times \mathbf{H}_R| = \gamma\beta M_s |\mathbf{H}_R| \sin\phi$ , where  $\phi$  is the DW tilting angle between  $+\hat{y}$  and  $\mathbf{M}$  at the DW center, and the experiment reported  $|\mathbf{H}_R| \sim 1\text{ T}$  at  $|\mathbf{j}_e| = 10^{12}\text{ A/m}^2$ . On the other hand, the magnitude of the nonadiabatic STT is  $\beta b_j |\partial\mathbf{M}/\partial x| \sim \beta b_j M_s/\lambda$ , where the DW width  $\lambda$  is about 5 nm and  $b_j = \mu_B P j_e / [e M_s (1 + \beta^2)]$  is of the order of 100 m/s at  $|\mathbf{j}_e| = 10^{12}\text{ A/m}^2$ . Thus the relative magnitude of the SL-STT with respect to the nonadiabatic STT is roughly given by  $\tilde{\alpha}_R \sin\phi$ , where the dimensionless parameter  $\tilde{\alpha}_R \equiv \pi\alpha_R m_e \lambda / \hbar^2 = (\pi/2)(\gamma\beta M_s |\mathbf{H}_R|) / (\beta b_j M_s / \lambda)$  is of the order of 10. Thus unless  $\phi$  is too small, the SL-STT can be indeed larger than the nonadiabatic STT and reverse the sign of  $v_{\text{DW}}$ .

Figures 3(a) and (b) show micromagnetic simulation results of Eq. (4) for the stable DW structure in Fig. 2(a). The inset in Fig. 3(a) shows  $v_{\text{DW}}$  as a function of  $\tilde{\alpha}_R$  at fixed  $j_e \equiv \hat{x} \cdot \mathbf{j}_e = +3 \times 10^{11}\text{ A/m}^2$  (amounting to  $b_j = +25\text{ m/s}$ ). Note that as  $\tilde{\alpha}_R$  increases,  $v_{\text{DW}}$  changes its sign from negative (along the electron flow direction) to positive (against the electron flow direction). The main panel in Fig. 3(a) shows  $v_{\text{DW}}$  as a function of  $j_e$  at two fixed values of  $\tilde{\alpha}_R$ , 0 (black squares) and 10 (red circles). For  $\tilde{\alpha}_R = 10$ ,  $v_{\text{DW}}$  changes from negative to positive at  $j_e \approx 3.5 \times 10^{11}\text{ A/m}^2$  and goes above +500 m/s for  $j_e > 1.5 \times 10^{12}\text{ A/m}^2$ . Thus both the anomalies (ii) and (iii) can be explained by RSOC if  $\tilde{\alpha}_R$  is sufficiently larger than 1. By the way, results for the DW structure in Fig. 2(b) are not shown since, when  $\tilde{\alpha}_R = 10$ , it is unstable and switches to the DW structure in Fig. 2(a) for  $j_e > 7.4 \times 10^{10}\text{ A/m}^2$ .

Next we demonstrate that the above explanation for the anomalies (ii) and (iii) does not work if the FL-STT is absent or very small. A recent experiment [13] on a somewhat different ultrathin magnetic system Pt/Co/Al reported that the SL-STT has a sizable magnitude but the FL-STT is negligibly small. This situation has been attributed [13] to a *perpendicular* spin current in Co generated from an *in-plane* charge current in the heavy metal layer (Pt) through the SHE. In the absence of the FL-STT, the stabilities of the two DW configurations in Fig. 2 are governed by the SL-STT. Recalling that the DW anisotropy energy of the Bloch DW favors  $\phi = 0$  and  $\pm 180^\circ$ , and disfavors  $\pm 90^\circ$ , it is evident that the SL-STT tends to destabilize/stabilize the DW structure in Fig. 2(a)/(b). Thus when the SHE-induced SL-STT is sufficiently strong, the DW structure in Fig. 2(b) is the only stable structure, which is opposite to the choice made by the FL-STT. Micromagnetic simulation for this

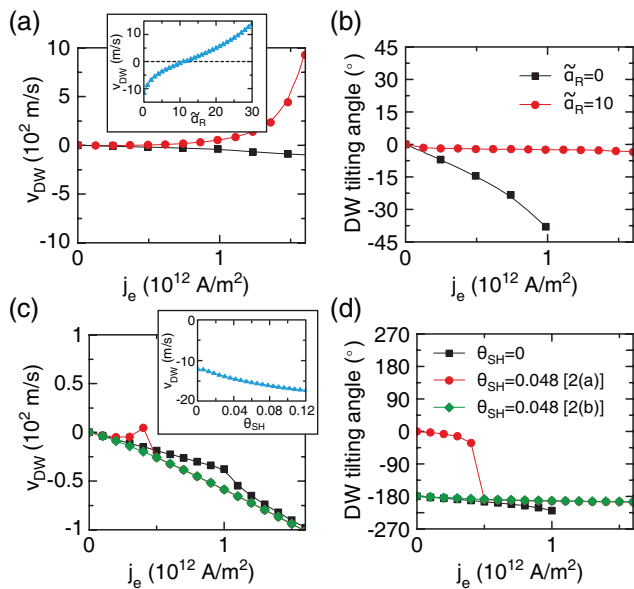


FIG. 3: (color online) Micromagnetic simulation results of the current-driven DW motion. In (a) and (b), RSOC effects are examined by using Eq. (4).  $v_{\text{DW}}$  (a) and the DW tilting angle  $\phi$  (b) [measured clockwise from  $+\hat{y}$  direction in Fig. 2(a)] as a function of  $j_e$  for  $\tilde{\alpha}_R = 0$  (black squares) and 10 (red circles). As shown in (b), the Walker breakdown is suppressed when  $\tilde{\alpha}_R = 10$  whereas it occurs for  $j_e > 1.0 \times 10^{12}$  A/m<sup>2</sup> when  $\tilde{\alpha}_R = 0$ . The inset in (a) shows  $v_{\text{DW}}$  as a function of  $\tilde{\alpha}_R$  for  $j_e = 3.0 \times 10^{11}$  A/m<sup>2</sup>. All results in (a) and (b) are for the stable DW configuration in Fig. 2(a). In (c) and (d), SHE effects are examined by setting  $\mathbf{H}_R = 0$  and instead adding to Eq. (4) the SHE-induced SL-STT  $\gamma \mathbf{M} \times [(\theta_{\text{SH}} \mathbf{M} / M_s) \times (H_S \hat{y})]$ , where  $H_S = \hbar j_{e,N} / (2e M_s t_F)$ ,  $t_F$  is the thickness of the ultrathin magnetic layer, and  $j_{e,N}$  is the charge current density in the heavy metal layer.  $j_{e,N} = j_e$  is assumed.  $v_{\text{DW}}$  (c) and  $\phi$  (d) as a function of  $j_e$  for  $\theta_{\text{SH}} = 0$  (black squares) and 0.048 [red circles and green diamonds for the DW structures in Figs. 2(a) and (b)]. Red circles are not visible for  $j_e > 5 \times 10^{11}$  A/m<sup>2</sup> since they overlap with green diamonds. The inset in (c) shows  $v_{\text{DW}}$  as a function of  $\theta_{\text{SH}}$  at  $j_e = 3.0 \times 10^{11}$  A/m<sup>2</sup> for the stable DW configuration in Fig. 2(b). The parameters for the simulation;  $\alpha = 0.5$ ,  $\beta = 0.25$  [23],  $M_s = 5.0 \times 10^5$  A/m, the perpendicular magnetic anisotropy constant  $K_u = 1.0 \times 10^6$  J/m<sup>3</sup>, the exchange stiffness constant  $A_{\text{ex}} = 1.0 \times 10^{-11}$  J/m,  $P = 0.7$ ,  $\gamma/2\pi = 28.0113$  GHz $\cdot$ T<sup>-1</sup>, and  $t_F = 0.6$  nm.

stable DW structure indicates [inset in Fig. 3(c)] that  $v_{\text{DW}}$  does not change its sign as  $\theta_{\text{SH}}$  grows, which is in contrast to the RSOC effect [inset in Fig. 3(a)]. Here  $\theta_{\text{SH}}$  is the spin Hall angle representing the strength of SHE. This result is natural since for the stable DW structure, the SL-STT is *parallel* to the nonadiabatic STT at the DW center. Note also that large enhancement of  $|v_{\text{DW}}|$  does not occur [Fig. 3(c)] either, since the SL-STT in Fig. 2(b) suppresses the deviation of  $\phi$  from  $\pm 180^\circ$ , thereby suppressing its own magnitude, which is proportional to  $\sin \phi$ . Thus SHE alone cannot explain the anomalies (ii) and (iii). By the way, the DW structure

in Fig. 2(a) may exhibit the sign-reversed  $v_{\text{DW}}$  [red circles in Fig. 3(c) near  $j_e = 4 \times 10^{11}$  A/m<sup>2</sup>] right before it loses its stability at  $j_e \approx 5 \times 10^{11}$  A/m<sup>2</sup> [downward jump of red circles by  $180^\circ$  in Fig. 3(d)]. However this sign-reversal should be contrasted with the sign-reversal observed [8] in the current range, where only one stable DW structure exists.

To conclude, we presented the theory of the RSOC-induced STTs, which explains various anomalous features of the magnetization dynamics in ultrathin magnetic systems. It will be valuable for future works to utilize ultrathin magnetic systems for next generation spintronic devices. Important future research directions include exploring other material combinations such as Ta/CoFeB/MgO, utilizing both RSOC and SHE to achieve enhanced properties, and understanding the dependence of the RSOC strength on magnetic layer thickness and material combinations. It is also interesting to explore possible connections between this work and other interesting phenomena in ultrathin magnetic systems such as magnetization control via electric voltage [24] and strong perpendicular magnetic anisotropy [6] in Ta/CoFeB/MgO systems. Lastly, during the preparation of this manuscript, we received a calculation [25], which also presents a derivation of the SL-STT but does not discuss implications of RSOC on the DW motion.

We gratefully acknowledge M. D. Stiles, R. McMichael, and W. Rippard for valuable comments. This work was financially supported by the NRF (2010-0014109, 2010-0023798, 2011-0030784, 2011-0028163) and BK21. KWK acknowledges the financial support by the NRF (2011-0009278).

\* Electronic address: kj'lee@korea.ac.kr

† Electronic address: hwl@postech.ac.kr

- [1] C. Chappert, A. Fert, and F. Nguyen Van Dau, *Nature Mater.* **6**, 813 (2007).
- [2] J. A. Katine and E. E. Fullerton, *J. Magn. Magn. Mater.* **320**, 1217 (2008).
- [3] J. C. Slonczewski, *J. Magn. Mag. Mater.* **159**, L1 (1996).
- [4] L. Berger, *Phys. Rev. B* **54**, 9353 (1996).
- [5] P. K. Amiri *et al.*, *IEEE Elec. Dev. Lett.* **32**, 57 (2011).
- [6] S. Ikeda *et al.*, *Nature Mater.* **9**, 721 (2010).
- [7] I. M. Miron *et al.*, *Nature* **476**, 189 (2011).
- [8] I. M. Miron *et al.*, *Nature Mater.* **10**, 189 (2011).
- [9] M. Hayashi *et al.*, *Phys. Rev. Lett.* **98**, 037204 (2007).
- [10] T. A. Moore *et al.*, *Appl. Phys. Lett.* **93**, 262504 (2008); *ibid.* **95**, 179902 (2009).
- [11] Y. A. Bychkov and E. I. Rashba, *J. Exp. Theor. Phys. Lett.* **39**, 78 (1984).
- [12] The mechanism of this term is related to a mechanism discussed in the context of a perpendicular current [K. M. D. Hals, A. Brataas, and Y. Tserkovnyak, *Europhys. Lett.* **90**, 47002 (2010)].
- [13] L. Liu, O. J. Lee, T. J. Gudmundsen, D. C. Ralph, and R. A. Buhrman, arXiv:1110.6846.

- [14] The correction to this approximation is ignored since it is not a response of an electric current.
- [15] S. Zhang and Z. Li, Phys. Rev. Lett. **93**, 127204 (2004).
- [16] When  $\mathbf{v}_{\pm}$  is not homogeneous, the spin diffusion dynamics modifies the relation between the spin current and the electric field [26] but it does not modify the RSOC-induced STTs expressed in terms of the current density.
- [17] A. Thiaville, Y. Nakatani, J. Miltat, and Y. Suzuki, Europhys. Lett. **69**, 990 (2005).
- [18] Y. Tserkovnyak, A. Brataas, and G. E. W. Bauer, J. Magn. Magn. Mater. **320**, 1282 (2008).
- [19] K. Obata and G. Tatara, Phys. Rev. B **77**, 214429 (2008).
- [20] A. Manchon and S. Zhang, Phys. Rev. B **78**, 212405 (2008); *ibid.* **79**, 094422 (2009).
- [21] I. M. Miron *et al.*, Nature Mater. **9**, 230 (2010).
- [22] J. Ryu, S.-M. Seo, K.-J. Lee, and H.-W. Lee, J. Mag. Mag. Mater. doi:10.1016/j.jmmm.2011.12.010.
- [23]  $\beta$  is assumed to be smaller than  $\alpha$  to be consistent with experiments [7, 8, 21];  $\alpha$  is about 0.5 [21]. We estimate  $\beta$  to be of order 0.1 in the experiments since the SL-STT [7] is about one order of magnitude smaller than the FL-STT [21] at the same current density. By the way, estimation of  $\beta/\alpha$  from  $v_{\text{DW}}$  is incorrect since RSOC strongly modifies  $v_{\text{DW}}$ .
- [24] Y. Shiota *et al.*, Nature Mater. **11**, 39 (2012); W.-G. Wang, M. Li, S. Hageman, and C. L. Chien, *ibid.* **11**, 64 (2012).
- [25] X. Wang and A. Manchon, arXiv:1111.1216.
- [26] K.-W. Kim, J.-H. Moon, K.-J. Lee, and H.-W. Lee, Phys. Rev. B **84**, 054462 (2011).